IOPscience iopscience.iop.org

Home Search Collections Journals About Contact us My IOPscience

Electronic and vibronic properties of n-type GaN: the influence of etching and annealing

This article has been downloaded from IOPscience. Please scroll down to see the full text article.

2002 J. Phys.: Condens. Matter 14 4461

(http://iopscience.iop.org/0953-8984/14/17/317)

View the table of contents for this issue, or go to the journal homepage for more

Download details:
IP Address: 171.66.16.104
The article was downloaded on 18/05/2010 at 06:34

Please note that terms and conditions apply.

INSTITUTE OF PHYSICS PUBLISHING JOURNAL OF PHYSICS: CONDENSED MATTER

J. Phys.: Condens. Matter **14** (2002) 4461–4476 PII: S0953-8984(02)32354-3

# Electronic and vibronic properties of n-type GaN: the influence of etching and annealing

**S Tripathy**[1,3], **S J Chua**[1,2] **and A Ramam**[2]

[1] Centre for Optoelectronics, Department of Electrical and Computer Engineering, National University of Singapore, 119260, Singapore
[2] Institute of Materials Research and Engineering, Lower Kent Ridge Road, Singapore

E-mail: elest@nus.edu.sg (S Tripathy)

Received 4 January 2002, in final form 18 March 2002
Published 18 April 2002
Online at stacks.iop.org/JPhysCM/14/4461

**Abstract**
We have investigated optical properties of the GaN etched surface using uv-micro-photoluminescence (PL) and micro-Raman scattering. The effects of wet chemical treatment (HCl and KOH) and $Cl_2$-based inductively coupled plasma etching on optical properties of n-type GaN have been studied. The damage introduced by dry etching was assessed and improvement of the band-edge PL was observed during post-etch annealing of the samples. The surface stoichiometry of the GaN surfaces subjected to different processing steps has been analysed based on the results of x-ray photoelectron spectroscopy. The atomic force microscopy technique is employed to investigate the surface morphology. Apart from phonons of GaN, Raman spectra also show impurity-induced local vibrational modes. In addition, electronic Raman peaks were observed in the low-frequency region. We have also carried out micro-Raman and PL measurements to investigate optical properties of n-type GaN annealed under different conditions. Biaxial strain and phonon lifetimes have been estimated in GaN subjected to various processing conditions.

## 1. Introduction

Due to enhanced mechanical strength, the ability to withstand high-temperature processing and chemical inertness, there is considerable attention towards the use of III nitrides for device fabrication. The electrical and optical properties of these materials are affected not only by the processes that occur during growth, but also by the post-growth processes that the materials undergo, such as surface treatment, thermal annealing and plasma etching. Despite technological advances, the generation of defects in GaN, their electronic properties and their effects on device properties are still unclear. During processing of GaN-based devices, it

[3] Author to whom any correspondence should be addressed.

© 2002 IOP Publishing Ltd Printed in the UK 

is difficult to identify which contributions belong to a given structural defect in the etched material where high density of dislocations, porous structures, point defects and impurities are present. Therefore, there is a need to improve the quality of the material during processing steps. Inductively coupled plasma (ICP) and reactive ion energy (RIE) etching have mostly been employed for the fabrication of GaN mesa structures [1–5]. ICP etching can provide low damage while maintaining fast etch rates and superior uniformity [6]. In addition to the higher etch rate, minimal modification of the surface material is desirable, which clearly indicates the importance of the study of post-etch material characterization for device fabrication. Optimized etching and annealing conditions will lead to better-quality GaN surfaces, which can be further used for fabrication of optoelectronic devices.

Photoluminescence (PL) spectroscopy has been used to investigate the effect of dry etching and annealing on luminescence properties of n-type GaN [7–10]. High-temperature annealing of GaN is also found to be an important processing step in the device fabrication of the LEDs, lasers and high-temperature electronic devices. As the $E_2$(TO) phonon frequency in GaN is sensitive to the lattice strain, Raman spectroscopy can be used as a powerful tool to investigate strain during high-temperature annealing of GaN-based materials. A convenient tool for impurity analysis is the study of their local vibrational modes (LVMs) through Raman spectroscopy [11–13]. In n-type GaN, a high concentration of silicon and oxygen may give rise to IR-active LVMs. Similarly, defect-correlated effects and interband transitions are also key sources of additional electronic and vibrational modes observed in GaN. Temperature-dependent Raman studies reveal the nature of these modes: whether of vibronic or electronic origin [14–17]. One of the fundamental aspects in device performance is the interaction of phonons with free carriers. The presence of decay channels shortens the lifetimes of phonons. This shortening is due to anharmonic interaction, impurities and defects [18]. Phonon lifetimes in GaN would be greatly affected during various processing conditions. A comprehensive Raman study of the dry-etched and annealed surface would reveal more information on the vibrational properties of GaN.

In this article, we report a systematic study of the effects of wet chemical treatment, ICP etching and annealing on surface and optical properties of n-type GaN. The n-GaN epitaxial layers grown by MOCVD are etched using $Cl_2/BCl_3$ plasmas and surface morphologies of the etched n-GaN are analysed by the AFM technique. Micro-Raman scattering has been used to probe the vibrational states of the GaN structures and provides information on the defects and strain in the dry-etched surface. Etch-induced damage was assessed from the PL intensity of the dry-etched surface and improvement of the luminescence properties was observed during post-etch annealing. We have also estimated lifetimes of phonons in n-type GaN subjected to various processing conditions.

## 2. Experiment

Si-doped GaN epitaxial layers of thickness 1.5–2.0 $\mu$m were grown in an EMCORE MOCVD reactor on (0001) sapphire substrates, with an undoped 25–30 nm buffer layer sandwiched in between. At room temperature (RT), the carrier concentration of the samples was found to vary in the range $2.1 \times 10^{18}$–$4.6 \times 10^{18}$. The as-grown GaN samples were cut into several pieces. A few pieces were treated with concentrated HCl (36%) for 5 min and then blown dry with $N_2$ and some other pieces were treated with boiling KOH solution for 5–6 min. For dry etching, planar structures were patterned by photolithography using AZ 5214 photoresist (PR) and were etched in the Plasma–Therm 770 system set at different ICP conditions. The ICP reactor was a load-locked Plasma–Therm SLR 770 set-up with the 2.0 MHz ICP source and configured with an electrode chuck in the chamber, which is biased separately at 13.56 MHz.

The patterned structures were exposed to $Cl_2/BCl_3$ plasmas. The etch rates of GaN and PR were obtained by measuring the patterned step before and after etching using the alpha-step profilometer. The operating pressure was kept constant at 5 mTorr during etching. The inductive power was kept at 500 W at a constant rf chuck power of 250 W. Increase in rf chuck power results in rough surface morphology. The $Cl_2/BCl_3$ gas flow rate was kept constant (16 sccm $BCl_3$ and 8 sccm $Cl_2$) during etching. The n-GaN etch rates in our samples were approximately 0.2 $\mu$m $min^{-1}$, and by choosing appropriate $Cl_2/BCl_3$ gas flow, ICP and rf chuck conditions, we obtained vertical and smooth etching profiles. To improve the optical quality, a few samples were also subjected to rapid thermal annealing (RTA) in a $N_2$ ambient for 2–3 min. Before RTA, the samples were treated with buffered HF solution for a minute. The surface morphology of the etched GaN surface was examined using a Topometrix AFM set-up operating in contact mode with a SiN tip. The PL spectra were recorded with a Renishaw 2000 micro-Raman-PL set-up. The 325 nm line of the He–Cd laser was used as a source of excitation. The chemical nature of the GaN surfaces was examined by x-ray photoelectron spectroscopy (XPS) on a VG ESSCALAB 220I-XL set-up using Mg K$\alpha$ radiation. The Ga:N ratio was evaluated by obtaining the normalized area under the curves of Ga(3d) and N(1s) peaks from the XPS high-resolution narrow scans, after subtracting a suitable background. The samples were also characterized by spatially resolved Raman scattering using the 514.5 nm line of an argon ion laser. The scattered light was dispersed through the JY-T64000 triple-monochromator system attached to a liquid-nitrogen-cooled CCD detector. The accuracy during the Raman measurements was 0.2 $cm^{-1}$, with a lateral spatial resolution of 1.2 $\mu$m. For low-temperature measurements, the samples were kept in a Linkam hot/cold stage, which is placed under the microscope of the Raman system. The temperature was measured by a K-type thermocouple with accuracy better than $\pm 1$ K. The instrumental linewidth was deconvoluted from the experimentally obtained values in order to obtain the true intrinsic linewidth of the phonon modes. In the dry-etched GaN surface, oxygen concentration in the range $10^{17}$–$10^{18}$ was measured by SIMS depth profiling. RTA of the as-grown samples was performed in the temperature range 500–1000 °C in an $O_2$ and $N_2$ environment.

## 3. Results and discussion

### *3.1. Surface morphology*

The surface morphology in terms of area root mean square (rms) roughness of the n-GaN films subjected to various processing steps was examined by AFM. The rms roughness was observed in the range 4–16 nm under varying processing conditions. Figure 1 shows the AFM micrographs of the samples subjected to different processing conditions. In order to obtain smooth GaN surface during high-density plasma etching, optimized conditions have been used to control the etch rate, selectivity, surface roughness and anistropy of the vertical sidewalls. Surface treatment and dry etching results in formation of numerous pyramidal structures. These structures are randomly distributed throughout the etched surface and may be developed due to the nanometre-scale intrinsic roughness. The surface inhomogeneities could be responsible for the variation in chemical resistance of GaN epilayers, which were subjected to etching in high-density plasmas. Wet etching and chemical treatment of n-GaN give rise to freestanding whiskers at the surface, 20–80 nm across, which are believed to contain dislocations. AFM data of the dry-etched surface show that etching results in surface inhomogeneties with a height difference of 20–30 nm. The micrographs also revealed the presence of some depressions and sub-micrometre hillocks, both within the 20 nm vertical range. Based on our AFM analysis of GaN grown on (0001) sapphire, the smooth surface is considered as Ga terminated. Hydrogen

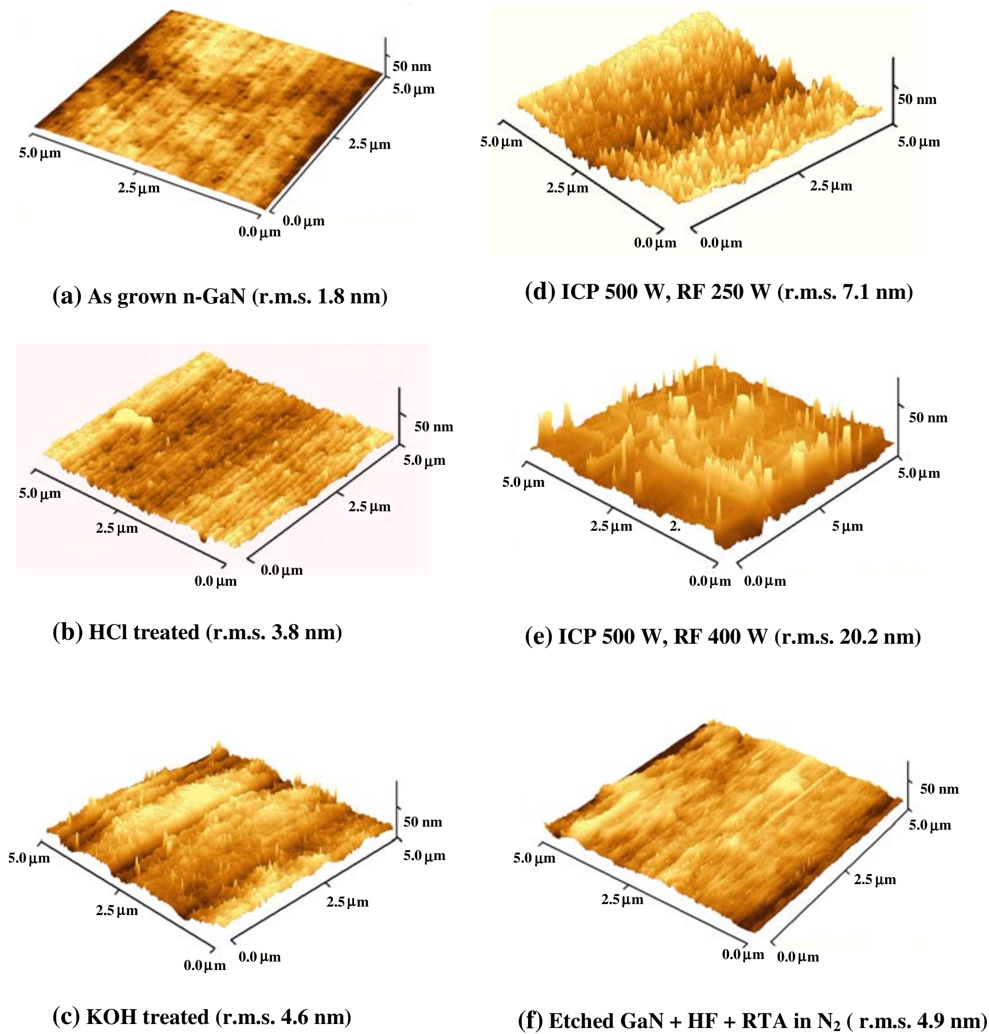


**Figure 1.** AFM micrographs ($5.0\times5.0\ \mu m^2$) of n-type GaN samples subjected to various processing steps. (*a*) As-grown GaN; (*b*) HCl-treated GaN; (*c*) KOH-treated GaN; (*d*) plasma-etched GaN using 500 W ICP, 250 W rf, 8 sccm $Cl_2$ and 16 sccm $BCl_3$; (*e*) plasma-etched GaN using 500 W ICP and 400 W rf; (*f*) plasma-etched GaN (500 W ICP and 250 W rf) subjected to HF treatment and RTA.

(This figure is in colour only in the electronic version)

adsorption during MOCVD growth influences the surface morphology of the as-grown film. However, during surface treatment and etching, preferential removal of Ga and N from the surface leads to formation of surface dangling bonds. The Ga-rich etched surface will lead to formation of occupied dangling-bond states and may give rise to surface states. These states are often passivated by oxygen termination. Removal of N from the surface would lead to unusual surface reconstruction by vacancy–impurity complexes during post-etch processing steps.

**Table 1.** Surface stoichiometry of GaN during different processing steps estimated from XPS data. The GaN surface compositions are normalized considering integrated intensity of the Ga(3d), N(1s), C(1s) and O(1s) peaks.

| Normalized surface composition | As-grown n-GaN | HCl treatment | KOH treatment | Dry-etched n-GaN (500 W ICP, 250 W RIE, and 33% $Cl_2$ in $Cl_2/BCl_3$) | Etched n-GaN subjected to HF treatment and RTA in $N_2$ ambient |
|---|---|---|---|---|---|
| Ga(%) 3d | $28.5 \pm 0.2$ | $34.3 \pm 0.2$ | $31.6 \pm 0.2$ | $23.3 \pm 0.2$ | $28.1 \pm 0.2$ |
| N(%) 1s | $17.2 \pm 0.2$ | $19.2 \pm 0.2$ | $21.3 \pm 0.2$ | $11.1 \pm 0.2$ | $16.3 \pm 0.2$ |
| C(%) 1s | $38.5 \pm 0.2$ | $36.1 \pm 0.2$ | $29.8 \pm 0.2$ | $34.8 \pm 0.2$ | $30.8 \pm 0.2$ |
| O(%) 1s | $15.6 \pm 0.2$ | $10.6 \pm 0.2$ | $17.0 \pm 0.2$ | $30.6 \pm 0.2$ | $24.6 \pm 0.2$ |
| Ga/N ratio | $1.6 \pm 0.1$ | $1.8 \pm 0.1$ | $1.5 \pm 0.1$ | $2.1 \pm 0.1$ | $1.7 \pm 0.1$ |

### *3.2. Surface stoichiometry*

The surface stoichiometry of the GaN samples subjected to various processing steps was studied by comparing the Ga(3d), Ga(2p), N(1s), C(1s) and O(1s) peaks in the XPS spectra. The Ga(3d) core level peak near 19 eV is mainly assigned to Ga–N-based chemical bonding. The N(1s) peak was observed near 398 eV. The chemical shift of the O(1s) peak observed near 533 eV represents the Ga–O bonding at the surface. The surface stoichiometry of the n-GaN subjected to surface treatment, ICP etching and post-etch annealing is shown in table 1. The compositions of elements were estimated from the normalized integrated intensity of the Ga(3d), N(1s), C(1s) and O(1s) peaks in the XPS spectra. The XPS chemical analysis shows that the surface of as-grown film is contaminated with carbon and oxygen. In as-grown GaN, a C(1s) peak occurs near 285 eV, which is typically a hydrocarbon contaminant in the GaN surface. XPS spectra from the samples subjected to dry etching and RTA show that there is no appreciable change of the total area under the C(1s) peak. However, the chemical shift of the C(1s) peak shows a reduction of carbon-related species after treatment with HCl and KOH. The Ga(2p) peak observed near 1120 eV in the as-grown films is found to be less intense after wet and dry etching and increases during annealing in nitrogen ambient. The Ga(3d) peak becomes more intense after etching. In addition, both Ga(3d) and Ga(2p) peaks show a chemical shift in binding energy. The most significant change is observed in the O(1s) peak. We found a decrease in the oxygen content after HCl treatment. XPS analysis also shows that the amount of oxygen increases in the dry-etched surface. KOH treatment shows a decrease in the carbon content from the surface. The C(1s) peak also shows a decrease in the etched surface after HF treatment and RTA. We have observed a shift in the binding energy of O(1s) after post-etch chemical treatment and RTA. We found that the atomic percentage of oxygen drops after HF treatment and post-etch annealing. A subsequent difference in the surface Ga-to-N ratio was also observed during such processing steps. The Ga-to-N ratio was evaluated by comparing the integrated intensities of the Ga(3d) and N(1s) peaks, taken from a single spectrum, over the entire binding energy range. The XPS analysis clearly shows that oxygen and carbon incorporation during processing introduces degradation of the luminescence characteristics in GaN by forming nonradiative recombination centres. It was necessary to remove the carbon and oxygen contents from the etched surface by wet chemical treatment and RTA.

To evaluate the quality of the surface-treated GaN films, micro-PL measurements were carried out. Figure 2 shows PL spectra of GaN before and after treatment with HCl and KOH solution. After HCl treatment, the intensity of the band edge peak decreases by 15% and that of the yellow luminescence (YL) peak decreases by 20%. With KOH treatment, there was appreciable increase of YL intensity. However, both treatments also correspond to some

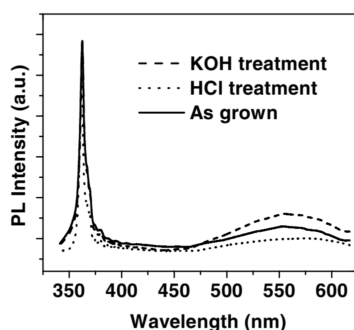


**Figure 2.** RT PL spectra of GaN subjected to HCl- and KOH-based wet chemical treatment. Surface treatment shows changes in the intensity of the YL transition in n-type GaN.

changes in the near-band-edge transitions. We conclude that HCl etching substantially etched gallium oxide from the surface but had no effect on carbon contaminants. As evident from XPS analysis, KOH treatment results in removal of carbon atoms, which could improve the contact properties of n-GaN. The surface states of the KOH-treated GaN may be dominated by vacancy–impurity complexes, which results in an increase of the YL intensity. We have seen that removal of surface oxide by HCl treatment correlates with a slight reduction of YL signal and related defect states. Such an assignment of YL to surface states and defects has also been described in the literature [19–21]. Our analysis shows that wet chemical treatment is effective in removing surface contaminants from the surface of the as-grown GaN layer. Since oxygen and carbon create a surface potential barrier and decrease the contact resistivity, surface treatment is a crucial step for improvement of metal contact properties.

### *3.3. Dry processing of n-GaN*

Micro-PL and Raman spectra from the dry-etched surface were recorded at RT. An area of more than $30 \times 30\ \mu m^2$ around the mesa structures was removed by dry etching to allow access to their optical properties without interference from the unetched area of the GaN surface. In the as-grown film, the carrier concentration was found to be $2.2 \times 10^{18}$ cm$^{-3}$ and decreases gradually from the etched surface. Figure 3 shows the PL spectra of dry-etched GaN subjected to various conditions. The band-edge PL intensity was found to decrease due to plasma-induced damage. Plasma-induced damage can be manifested in different forms, all of which may affect the electronic and optical properties of devices fabricated on the etched materials. Damage may occur due to deposition of the polymer, creation of non-stoichiometric surfaces due to preferential depletion of one of the elements and creation of near-surface lattice defects, which can diffuse deep into the etched surface. Recently, vacancy effects on plasma-induced damage in n-type GaN have been addressed by Chua *et al* [22]. In this study, the etch-induced damage of GaN has been evaluated in ICP plasma conditions using PL and Raman measurements. The near-band-edge transitions in these RT PL spectra were observed near 363 nm. The broad YL from the samples was centred around 560 nm. Due to variation in the surface roughness, the change in PL intensity from different positions of the samples was monitored using our micro-PL set-up. No significant change was noted in the band-edge PL signal throughout the etched surface. There was a small increase in FWHM in the dry-etched samples.

In the etched GaN surface, under identical electronic excitations, the ratio of the band-edge to YL peak intensity can be used as a figure of merit indicating the quality of the etched surface. We have observed considerable change in the integrated PL intensity ratio of the

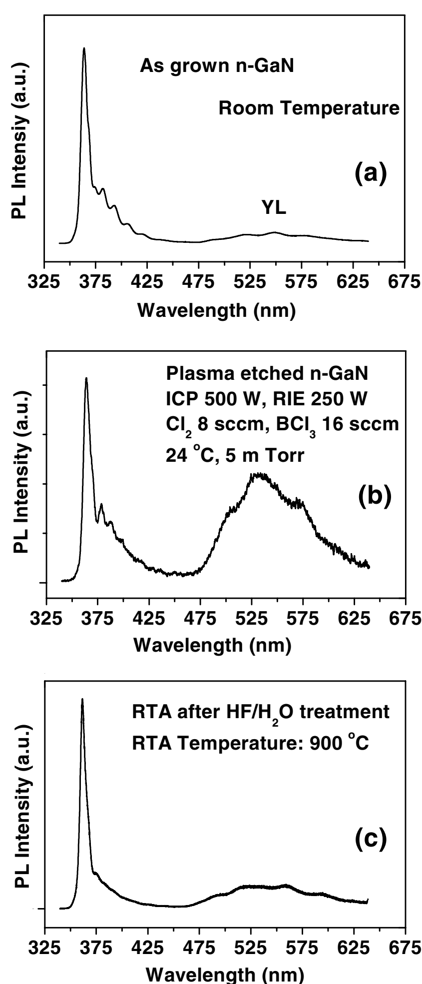


**Figure 3.** RT PL spectra of GaN subjected to various processing steps: (*a*) as-grown GaN; (*b*) plasma-etched GaN with 500 W ICP, 250 W RIE power, 8 sccm $Cl_2$ and 16 sccm $BCl_3$; (*c*) etched GaN film subjected to RTA in $N_2$ at 900 °C after HF/$H_2O$ treatment.

band-edge and YL transitions. The spectra from the etched surface show that the intensity of the band-edge peak decreases to 30–40% of its as-grown value. More than 25% increase of the YL intensity was observed from the etched samples. During plasma etching, nitrogen depletion occurs and may result in formation of more nitrogen vacancies at the surfaces with gallium-rich layers. Previous XPS studies show enhancement of oxygen incorporation in etched GaN surfaces [23]. Increase in ion bombarding energy may influence the formation of donors and deep acceptor states near the surface. Similarly, etching under $Cl_2/BCl_3$ chemistry may increase the formation of $GaCl_3$ and $NCl_3$ as etch products. In some cases, such processing might result in a Ga-deficient surface due to removal of gallium forming $GaCl_3$. The presence of a higher concentration of reactive Cl will initiate changes in the surface stoichiometry and lead to formation of traps or point defects. The traps act as a source for native defects or impurities. The gallium vacancy $V_{Ga}$ is the most favourable native deep acceptor and this vacancy can form a complex with the nearest-neighbour $O_N$ and a less stable complex with the

second-neighbour $Si_{Ga}$. ($V_{Ga}$–$O_N$) and ($V_{Ga}$–$Si_{Ga}$) complexes have low formation energies and are, therefore, expected to play significant roles in YL generation [24–26]. Considering the low formation energy of $V_{Ga}$–$O_N$, it is suggested that oxygen contaminants enhance the formation of Ga vacancies during growth and processing. Positron experiments reveal a high concentration of Ga vacancies in nominally undoped and n-type GaN where the conductivity is due to unintentional oxygen incorporation [27]. The results show that the presence of oxygen donors in GaN promotes the formation of Ga vacancies and leads to the creation of these $V_{Ga}$–$O_N$ complexes. The concentration of Ga vacancies has been found to correlate with the intensity of YL [28]. Exposing the samples to air after etching implies oxygen termination and formation of $O_N$ complexes near the surface. The increased probability of $V_{Ga}$–$O_N$ complex formation and related shallow-donor–deep-acceptor transitions will lead to further enhancement of the YL from the etched surface.

We can conclude that there may be creation of surface contaminants such as O and C during etching, thermal annealing and post-etch processing conditions. Oxygen termination is likely to occur before chemical treatment and RTA. Dry etching of the patterned samples using a PR mask could lead to formation of carbon traces on the surface, which are difficult to remove with acetone and ultrasound cleaning. RTA of the etched surface in $N_2$ resulted in an improved Ga:N ratio and indicates replacements of Ga–O bonds by Ga–N bonding at the surface. However, during annealing, there is a possibility of formation of carbon-induced nonradiative recombination centres. Therefore, before RTA, the etched sample was treated with HF/$H_2O$ solution. After HF treatment and RTA the shift of the Ga(3d) peak towards lower binding energy represents stronger Ga–N bonding. Thus, post-etch chemical treatment and annealing in $N_2$ ambient is found to be effective in removing surface oxide and other carbon-containing contaminants. Such post-etch processing will also reduce the concentration of other species such as Cl-based contaminants and consequently improves the PL performance. Post-etch HF treatment and RTA in $N_2$ environment shows reduction of YL intensity and considerable enhancement of band-edge transitions. A sharp increase in the band-edge PL intensity at temperature 900 °C during post-etch annealing was observed as shown in figure 3(*c*). A decrease in the magnitude of the YL transition is also clearly observed. The overall decrease of the YL peak (30–50%) with HF/$H_2O$ treatment and RTA confirms that oxygen atoms are the main cause of the YL.

Raman spectra were recorded at different locations and under different plasma conditions from the dry-etched pattern. The Raman intensity in the spectra was compared to investigate the plasma-induced damage introduced into GaN. RT and 80 K Raman spectra of the n-GaN sample subjected to various processing steps are shown in figure 4. The spectra show Raman-active $A_1$(LO) and $E_2$(TO) phonons near 734 and 569 cm$^{-1}$ allowed by the $z(xx)\bar{z}$ scattering geometry. Cross-sectional measurements show additional modes of wurtzite GaN such as $A_1$(TO) (534 cm$^{-1}$), $E_1$(TO) (560 cm$^{-1}$) and $E_1$(LO) (742 cm$^{-1}$). The sapphire $A_{1g}$ and $E_{1g}$ modes from the samples were observed near 418 and 750 cm$^{-1}$, respectively. Due to damage introduced into the GaN surface, the Raman signal decreases from the etched surface. A close inspection of various phonon modes from the etched surface shows a shift of phonon frequency by 1–2 cm$^{-1}$ towards the higher-energy side from the as-grown region. From the samples, we have also found several lines in the low-frequency region at low temperature, and the intense lines are located at 99, 210 and 240 cm$^{-1}$. The disorder-activated modes are observed near 150 and 300 cm$^{-1}$. In the high-frequency region, we have observed additional modes near 546, 675 and 690 cm$^{-1}$ from the dry-etched surface. Considering phonon dispersion of GaN and sapphire, the low-energy Raman lines cannot be associated with phonon modes from GaN and sapphire. Therefore, these distinct lines may arise from defects incorporated into GaN during growth and processing and are visible due to their vibronic or electronic excitations.

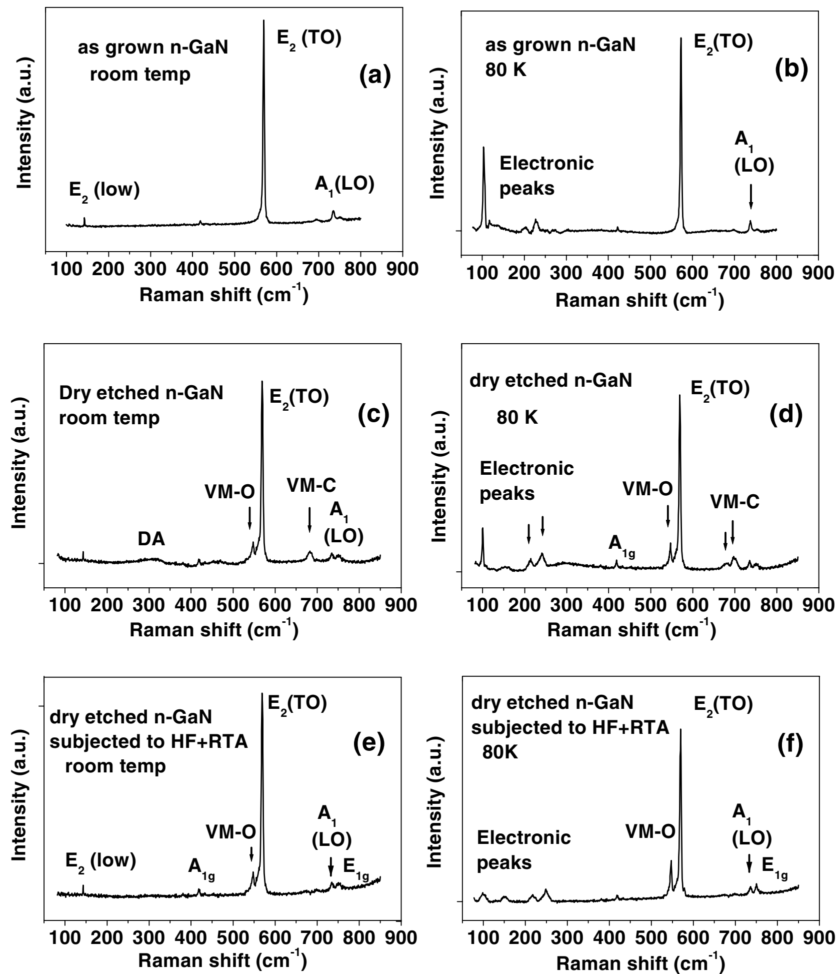


**Figure 4.** RT and 80 K micro-Raman spectra of GaN subjected to various processing conditions ($z(xx)\bar{z}$ geometry). (*a*) Spectra of as-grown GaN at RT; (*b*) spectra of as-grown GaN at 80 K; (*c*) spectra of dry-etched GaN at RT; (*d*) spectra of dry-etched GaN at 80 K; (*e*) RT Raman spectra of plasma-etched GaN treated with HF and annealed in $N_2$ at 900 °C; (*f*) 80 K Raman spectra of plasma-etched GaN treated with HF and annealed in $N_2$. The vibronic and electronic peaks in the spectra are marked with arrowheads (↓).

Observation in the Raman spectra at 300 cm$^{-1}$ were reported by Limmer *et al* [29], where they have interpreted the mode as resulting from the damage of the crystal lattice induced by the post-growth ion implantation. They have also assigned modes near 670 cm$^{-1}$ to vacancy-related defect LVMs. In figure 4, the peaks at 150 and 300 cm$^{-1}$ are assigned to disorder-activated scattering, in which built-in defects, due to loss of translational symmetry, yield a relaxation of the $\boldsymbol{q} = 0$ selection rules for the first-order Raman scattering.

Several authors have reported LVMs in GaN in the frequency region 100–800 cm$^{-1}$ [30,31]. Electronic Raman peaks near 189 cm$^{-1}$ (23.4 meV), 237 cm$^{-1}$ (29.4 meV), 151 cm$^{-1}$ (18.7 meV) and 217 cm$^{-1}$ (26.9 meV) have been reported by Ramsteiner *et al* [14]. Siegle *et al* [16] found impurity-induced modes in GaN near 95, 125, 150, 190, 220, 235 and 250 cm$^{-1}$ and showed that the modes are of vibronic origin rather than electronic. In their report, the modes near 190 and 235 cm$^{-1}$ were attributed to a defect cluster based on their linewidth. In the

low-temperature spectra shown in figure 4, the peak near 99 $cm^{-1}$ can be assigned to a defect-induced quasi-local vibrational mode [15]. In addition, we observed modes near 546 $cm^{-1}$ from the etched surface (assigned as VM–O in figure 4) in $z(xx)\bar{z}$ and $x(zz)\bar{x}$ geometries. Reports of phonon quasi-modes in this range between $A_1$(TO) and $E_1$(TO) modes reveal that such a mode would appear parallel to the TO modes due to polarization breakdown and it should be broader than either of the TO modes [32]. The polarization conditions show no sign of phonon quasi-modes. The correlation of the mode near 546 $cm^{-1}$ and high concentration of oxygen in the etched surface suggest that such modes could be the vibrational modes of O donors, substituted on the N site in GaN. Wetzel *et al* [13] recently observed such vibrational modes near 544 $cm^{-1}$ in oxygen-doped GaN. On the higher-energy side, we have also observed modes near 675 and 690 $cm^{-1}$ in $z(xx)\bar{z}$ and $x(zz)\bar{x}$ scattering configurations. The behaviour of such modes with temperature shows that these lines may occur due to a vibrational or electronic Raman scattering of defects generated during processing. The small mass difference between C and N atoms causes C-induced modes with frequencies close to those of phonons of the perfect host crystal. According to [31], the C-induced modes are expected near 600 $\pm$ 8, 606 $\pm$ 10, 678 $\pm$ 2, 715 $\pm$ 3 and 744 $\pm$ 17 $cm^{-1}$. We have assigned the modes near 675 and 690 $cm^{-1}$ as carbon-induced vibrational modes (assigned as VM–C in figure 4), which are active due to the electronic transition associated with the $C_N$ complexes. These modes also show significant intensity reduction in the etched surface subjected to HF treatment and RTA.

The YL observed from the processed samples is due to the recombination of different shallow donors with a deep acceptor. The observation of various Raman lines and their temperature dependence clearly shows that the donors related to oxygen, silicon or carbon might have different ionization energies. Such electronic Raman lines can be associated with inner transitions of different donor species (1s–2s and 1s–3s transitions). The excitable donor and acceptor energies are different due to different electronic structures resulting from oxygen, carbon and silicon-like donors and deep-gap acceptors. For the low-energy Raman lines, we consider electronic Raman scattering, which controls the Raman intensity variation with temperature through thermal excitations of the electronic states. Ionization energy of 32–36 meV has been reported for oxygen donors in GaN (O donor substituted for nitrogen: $O_N$) [33, 34] and that for silicon in the range 16–32 meV [35, 36]. The low-energy lines can be related to such electronic excitations of silicon and oxygen donors. The micro-Raman spectra of a few dry-etched samples also exhibit the allowed high-frequency $A_1$ LO-phonon–plasmon (LPP) mode along with the $E_2$(TO) mode. Due to the etched surface orientation, symmetry-forbidden modes such as the $E_1$(TO) and $A_1$(TO) mode also occur near 560 and 534 $cm^{-1}$, respectively. The $LPP^+$ mode occurs in the high-frequency region and centred around 1050 $cm^{-1}$ and is extremely broad. The carrier concentration calculated from the LPP mode ($1.2 \times 10^{18}$ $cm^{-3}$) was found to agree with the Hall measurements. Post-etch chemical treatment and RTA result in enhancement of the intensity of all the Raman-active modes of GaN. Such a post-etch procedure improves the optical quality of the dry-etched material.

### *3.4. Thermal annealing*

To study the effect of thermal annealing on optical properties, we have carried out PL measurements on GaN samples annealed under different environment. The as-grown GaN samples were subjected to RTA in $N_2$and $O_2$ ambient. The PL spectra of the annealed n-type GaN samples are shown in figure 5. The RT spectra are dominated by the band-edge transition at 3.39 eV. 80 K PL peaks are dominated by near-band-edge excitonic transitions near 358.3 nm (3.460 eV) and 362.1 nm (3.424 eV). From the analysis of temperature-dependent PL spectra (80–300 K), the peak near 3.460 eV at 80 K can be related to a free-exciton (FX) transition.

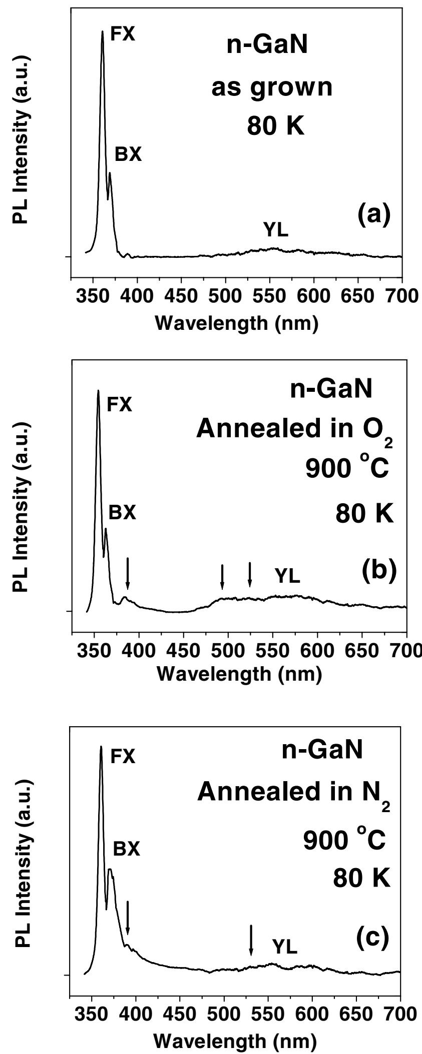


**Figure 5.** 80 K PL spectra of n-type GaN samples annealed under various conditions. (*a*) PL spectra of as-grown GaN; (*b*) PL spectra of GaN annealed in $O_2$ambient at 900 °C and (*c*) PL spectra of annealed GaN in $N_2$ ambient at 900 °C. Defect-induced PL bands are marked with arrowheads (↓).

The PL peak near 3.424 eV disappears when the temperature of the sample exceeds 150 K and represents a bound-exciton (BX) transition. Moreover, these two exciton lines retain the same relative intensity from the as-grown material through the different annealing treatments. Therefore, the 80 K PL peak near 3.424 eV could be associated with Si donors in n-type GaN. Additional peaks near 383.6 nm (3.232 eV) and 482.3 nm (2.57 eV) were also observed in the annealed samples. The defect-related YL bands are seen near 2.25 eV. PL spectra of samples in different annealing conditions show that the band-edge intensity is more enhanced in $N_2$ than in $O_2$. From the relative intensity of the band-edge PL peaks, we found that annealing in $N_2$ shows enhancement of the PL intensity over the as-grown GaN. In addition, the ratio of the integrated intensity of band-edge to YL transition increases while annealing in $N_2$. Annealing in $O_2$ shows degradation of the band-edge intensity over the as-grown GaN and a decrease

in the ratio of the integrated intensity of the band-edge to YL transition. The appearance of defect-related bands was seen in samples with higher YL signal. We have observed a shift in PL spectra by 15–20 meV upon annealing. The transition near 3.232 eV can be associated with an exciton bound to a stacking fault or an acceptor [37–40]. The movement of misfit dislocations during annealing can create stacking faults. The shift of PL peaks towards the lower-energy side implies strain relaxation upon annealing. The appearance of the peaks near 3.232 and 2.57 eV after annealing in oxygen suggests that oxygen impurities may be involved in the transition. With change in the excitation laser power, we have also observed spectral changes of the peak near 2.3 and 2.57 eV. Due to the change of excitation intensity, the corresponding change appears in the PL signal of the defect-related transition. The modes at 2.3 and 2.57 eV can be related to shallow-donor–deep-acceptor transitions. In one case this is the $O_N$-to-$V_{Ga}$ transition (deep level) while in another case it may be associated with an acceptor-like native defect $C_N$. The intensity of the deep-level bands near 2.3 and 2.57 eV increased due to increase in defect concentration. The surface roughness of the GaN layer increases drastically during high-temperature annealing. Annealing in different ambients shows a variation of rms roughness from 2 to 12 nm. Due to high-temperature annealing, atoms near the surface become mobile and crystal regrowth can occur due to activation processes. Depending on the shape and size, each columnar grain will have a different amount of the lattice strain during annealing. At higher temperature, the surface becomes smooth due to the sublimation process. Annealing in oxygen favours the formation of reactive oxygen atoms or OH radicals and results in the inclusion of oxygen as gallium oxide at the grain boundaries and surfaces. However, high-temperature annealing in nitrogen ambient seems reasonable for processing. The XPS data also show that the Ga/N ratio (surface stoichiometry) improves upon annealing in an $N_2$ environment.

### *3.5. Biaxial strain and phonon lifetimes*

We have found changes of the Raman peaks and lineshape from the etched surface of GaN. In a few samples, we have also seen the appearance of cracks along the mesa structures during ICP etching of GaN. The position-dependent stress measurement in the mesa pattern was studied along etched and unetched regions of the patterned structures. We found that biaxial stress is larger at the interface along the mesa structures than that of the as-grown layer. Annealing of the as-grown samples in nitrogen ambient leads to phonon softening and relaxation of biaxial strain. The biaxial stress was calculated and is shown in table 2 for GaN subjected to various processing conditions. A 400 $\mu$m HVPE-grown GaN layer is assumed to be strain free and the $E_2$(TO) phonon from this sample was observed near 567.5 cm$^{-1}$. The biaxial stress was calibrated from the frequency shift of the $E_2$(TO) mode: $\Delta\omega = (4.2 \pm 0.3)\sigma_{xx}$ cm$^{-1}$ GPa$^{-1}$, where $\sigma_{xx}$ is the in-plane biaxial stress [41]. Neglecting anisotropic relaxation, the strain versus stress relations using the set of stiffness constants can be given by

$$e_{xx} = \left[\frac{1}{C_{11} + C_{12} - 2(C_{13}^2/C_{33})}\right]\sigma_{xx}. \qquad (1)$$

The values of elastic stiffness constants $C_{ij}$ were taken from [42]. From micro-Raman observations, we have found that the stress analysis is independent of the shape and size of the nanostructures formed on the etched surface. The deviation of stress in the spatial dimensions of the surface inhomogeneities, i.e. in the nanometre scale, smoothed out within the spatial resolution and probing depth of micro-Raman measurements.

From micro-Raman mapping of strain, we have found that during annealing compressive stress is dominant in an $O_2$ environment rather than an $N_2$ ambient. Table 2 also lists the

**Table 2.** Biaxial strain and stress in GaN subjected to dry processing and annealing in $O_2$ and $N_2$ ambient.

| | | Dry processing | | Thermal annealing of the as-grown Si-doped GaN | | | | | |
|---|---|---|---|---|---|---|---|---|---|
| | | | | $O_2$ ambient | | | $N_2$ ambient | | |
| Properties | As grown n-GaN | Plasma etched | Post-etch HF + RTA in $N_2$ | 600 °C | 900 °C | 1000 °C | 600 °C | 900 °C | 1000 °C |
| 80 K FX PL peak (eV) | 3.460 | 3.476 | 3.462 | 3.464 | 3.474 | 3.480 | 3.466 | 3.454 | 3.442 |
| $E_2$(TO) ($cm^{-1}$) | 569.2 | 570.4 | 568.6 | 569.7 | 570.8 | 571.2 | 569.6 | 568.4 | 566.9 |
| In-plane strain ($e_{xx}$) | −0.0008 | −0.0013 | −0.0005 | −0.0010 | −0.0015 | −0.0017 | −0.0009 | −0.0004 | +0.0002 |
| In-plane stress $\sigma_{xx}$ (GPa) | −0.40 | −0.69 | −0.26 | −0.52 | −0.78 | −0.88 | −0.49 | −0.21 | +0.14 |

frequency position of the $E_2$(TO) phonon and in-plane strain tensor component in GaN as a function of the annealing temperature for different ambients. The frequency of the $E_2$(TO) phonon is very sensitive to strain whereas that of the $A_1$(LO) phonon depends on strain as well as on the free-carrier concentration. Annealing in $O_2$ ambient results in an increased $E_2$(TO) phonon frequency, which probes compressive strain during annealing. The maximum frequency shift was observed at 1000 °C. The results show that inclusion of oxygen into GaN is responsible for the strain introduced during high-temperature processing. No systematic shift was observed during annealing in an $N_2$ environment. The linewidth of the $E_2$ phonon increases during annealing in oxygen and no significant change in $N_2$ ambient was observed. Annealing in $N_2$ above 1000 °C reduces the linewidth but results in poor surface morphology. Though the as-grown GaN is under compressive strain, high-temperature annealing in $N_2$ at 1000 °C shows that the GaN nucleation layer becomes tensile. The strain relaxation during high-temperature annealing can be attributed to the extended domain matching mechanism [43]. At high temperature, the in-plane crystal domain grows due to increased mobility of the deposited atoms. As the domain size exceeds a few atomic distances, the extended domain matches the in-plane epitaxy of the epilayer with that of the sapphire substrate. Such a process would lead to a change in the stress value. Micro-Raman spectra were also recorded at different temperatures. The temperature dependence of the optic modes can be attributed to the anharmonic terms in the vibrational potential energy, which leads to a decay of the optical phonon into two, three or more low-energy phonons, respectively, from cubic, quartic or higher-order anharmonicities [44–46]. Temperature-dependent Raman spectra from the surface of etched and post-annealed GaN were analysed in the temperature range 80–500 K. As expected, we observed a decrease in the line width and a shift in the line centre towards higher frequencies as the temperature is lowered to 80 K. In the etched GaN film, the shift of 3–4 $cm^{-1}$ can be associated with an additional strain component.

Next, we estimate phonon lifetimes in GaN. The major contribution towards phonon lifetimes originates from anharmonic interactions in which a phonon decays into other lower-energy phonons. The phonon scattering at impurity or defect centres results in inhomogeneous broadening of the Raman lines. The analysis of the linewidth broadening in the Raman spectra can be used as an indirect measurement to estimate the lifetime of the first-order optical phonon at the Brillouin-zone centre. We have noted lifetime shortening in the GaN samples subjected to dry etching. Assuming a Lorentzian function for the deconvoluted line shape of the natural

**Table 3.** Lifetimes of phonons at RT estimated from equation (2) in n-type GaN subjected to various processing conditions.

| Phonons | Lifetimes of phonons (ps) | | | | | |
|---|---|---|---|---|---|---|
| | As grown | Surface treated (HCl) | Dry etched | Dry-etched GaN + (HF treatment) + (RTA in $N_2$) | As-grown GaN annealed in $O_2$ (900 °C) | As-grown GaN annealed in $N_2$ (900 °C) |
| $E_2$(TO) | 2.21 | 2.42 | 1.88 | 1.62 | 1.34 | 1.92 |
| $A_1$(LO) | 0.94 | 1.16 | 0.82 | 0.73 | 0.62 | 0.98 |

Raman line, the lifetimes '$\tau$' of the phonons are calculated from the energy–time uncertainty relation [18, 47],

$$\frac{1}{\tau} = \frac{\Delta E}{\hbar} \tag{2}$$

where $\Delta E$ is the Raman linewidth of the first-order optical mode in $\mathrm{cm}^{-1}$ at zero slit width, and $\hbar = 5.3 \times 10^{-12}\ \mathrm{cm}^{-1}$ s. From the RT measurements in the etched GaN region, the present method yields values of $\tau$ of 9.2, 0.78, 1.62, 1.88 and 0.82 ps for $E_2^{low}$(TO), $A_1$(TO), $E_1$(TO), $E_2^{high}$(TO) and $A_1$(LO) modes, respectively. Table 3 summarizes the calculated lifetimes of phonons in GaN subjected to various processing steps. Due to removal of surface oxides by HCl treatment, we have observed increases in the values of $E_2$(TO) and $A_1$(LO) lifetimes. In the etched GaN material containing impurities, additional channels of phonon decay may take place. Due to the presence of defects, dislocations and impurities, these imperfections can reduce the translational symmetry of the crystal, and thus perturb the characteristic lifetimes of propagating phonons. The lifetime of the LO phonon is often dominated by a three-phonon process, where the LO mode decays into a TO and an LA mode and the decay results in a more reasonable lifetime of a few picoseconds. Similarly, the lifetime of the $E_2$(TO) phonon is dominated by a four-phonon process, where the TO mode decays into $E_2^{low}$(TO) and two TA modes. The model has been supported by time-resolved and temperature-dependent Raman measurements [48–50]. The presence of impurities and surface states leads to phonon lifetime shortening in GaN subjected to dry processing. Due to improvement of the optical quality of GaN by wet chemical treatment and RTA, we have observed changes in the phonon lifetimes compared with the plasma-etched surface. Thermal annealing also leads to changes in the values of lifetime of $E_2$(TO) and $A_1$(LO) phonons.

## 4. Conclusions

We have carried out a detailed study of the effects of surface treatment, ICP etching and thermal annealing on the surface and optical properties of n-type GaN. HCl- and KOH-based wet chemical treatment is effective to remove surface contaminants and such treatment can improve the electrical and optical properties of the material. The Si-doped GaN epitaxial layers were etched using $Cl_2/BCl_3$ plasmas. The surface morphology and stoichiometry of the films have been analysed by AFM and XPS techniques. Post-etch chemical treatment and high-temperature annealing in $N_2$ are effective in improving optical properties of the etched surface. The micro-Raman spectrum from the etched surface shows the appearance of vibrational modes in n-type GaN. In addition, electronic Raman peaks are also observed in GaN subjected to various processing conditions. The $E_2$(TO) phonon frequency, being sensitive to the lattice strain, allowed Raman spectroscopy as a tool to investigate strain during etching

and annealing of GaN. We have also estimated phonon lifetimes in n-type GaN subjected to various processing conditions.

## Acknowledgments

This work was financially supported by the Singapore Agency for Science, Technology and Research (A*STAR) and Fujitsu Quantum Devices Singapore (FQDS). Dr J S Pan (IMRE) is acknowledged for his help in XPS measurements.

## References

[1] Lin M E, Fan Z F, Ma Z, Allen L H and Morkoc H 1994 *Appl. Phys. Lett.* **64** 887
[2] Pearton S J, Abernathy C R, Ren F and Lothian J R 1994 *J. Appl. Phys.* **76** 1210
[3] Lee H, Oberman D B and Harris J S Jr 1995 *Appl. Phys. Lett.* **67** 1754
[4] McLane G F, Casas L, Pearton S J and Abernathy C R 1995 *Appl. Phys. Lett.* **66** 3328
Cho H, Vartuli C B, Donovan S M, Abernathy C R, Pearton S J, Shul R J and Constantine C 1998 *J. Vac. Sci. Technol.* A **16** 1631
Im Y H, Park J S, Hahn Y B, Nahm K S, Lee Y S, Cho B C, Lim K Y, Lee H J and Pearton S J 2000 *J. Vac. Sci. Technol.* A **18** 2169
[5] Nakamura S 1997 *GaN and Related Materials* ed S J Pearton (New York: Gordon and Breach)
[6] Pearton S J, Zolper J C, Shul R J and Ren F 1999 *J. Appl. Phys.* **86** 1
[7] Cheung R, Withanage S, Reeves R J, Brown S A, Ben-Yaacob I, Kirchner C and Kamp M 1999 *Appl. Phys. Lett.* **74** 3185
[8] Cheung R, Reeves R J, Brown S A, Van der Drift E and Kamp M 2000 *J. Appl. Phys.* **88** 7110
[9] Hayes J M, Kuball M, Bell A, Harrison I, Korakakis D and Foxon C T 1999 *Appl. Phys. Lett.* **75** 2097
[10] Bell A, Harrison I, Korakakis D, Larkin E C, Hayes J M, Kuball M, Grandjean N and Massies J 2001 *J. Appl. Phys.* **89** 1070
[11] Kaschner A, Siegle H, Kaczmarczyk G, Straßburg M, Hoffmann A, Thomsen C, Birkle U, Einfeldt S and Hommel D 1999 *Appl. Phys. Lett.* **74** 3281
[12] Harima H, Inoue T, Nakashima S, Ishida M and Taneya M 1999 *Appl. Phys. Lett.* **75** 1383
[13] Wetzel C, Amano H, Akasaki I, Ager J W III, Grzegory I, Topf M and Meyer B K 2000 *Phys. Rev.* B **61** 8202
[14] Ramsteiner M, Mennniger J, Brandt O, Yang H and Ploog K H 1996 *Appl. Phys. Lett.* **69** 1276
[15] Seigle H, Kaschner A, Hoffmann A, Broser I, Thomsen C, Einfeldt S and Hommel D 1998 *Phys. Rev.* B **58** 13 619
[16] Jiang D, Ramsteiner M, Ploog K H, Tews H, Graber A, Averbeck R and Riechert H 1998 *Appl. Phys. Lett.* **72** 365
[17] Tripathy S, Soni R K, Asahi H and Gonda S 2000 *Physica* B **275** 301
[18] Bergman L, Alexson D, Murphy P, Nemanich R, Dutta M, Stroscio M, Balkas C, Shin H and Davis R F 1999 *Phys. Rev.* B **59** 12 977
[19] Shalish I, Kronik L, Segal G, Shapira Y, Zamir S, Meyler B and Salzman J 2000 *Phys. Rev.* B **61** 15 573
[20] Brown S A, Reeves R J, Haase C S, Cheung R, Kirchner C and Kamp M 1999 *Appl. Phys. Lett.* **75** 3285
[21] Shalish I, Shapira Y, Burstein L and Salzman J 2001 *J. Appl. Phys.* **89** 390
[22] Chua S J, Choi H W, Zhang J and Li P 2001 *Phys. Rev.* B **64** 205302
[23] Choi H W, Chua S J, Ramam A, Pan J S and Wee A T S 2000 *Appl. Phys. Lett.* **77** 1795
[24] Toth M, Fleischer K and Phillips M R 1999 *Phys. Rev.* B **59** 1575
[25] Neugebauer J and Van de Walle C G 1996 *Appl. Phys. Lett.* **69** 503
[26] Mattila T and Nieminen R M 1997 *Phys. Rev.* B **55** 9571
[27] Oila J *et al* 2001 *Phys. Rev.* B **63** 045205
[28] Saarinen K *et al* 1997 *Phys. Rev. Lett.* **79** 3030
[29] Limmer W, Ritter W, Sauer R, Mensching B, Liu C and Rauschenbach B 1998 *Appl. Phys. Lett.* **72** 2589
[30] Kasic A, Schubert M, Einfeldt S, Hommel D and Tiwald T E 2000 *Phys. Rev.* B **62** 7365
[31] Kaczmarczyk G, Kaschner A, Hoffmann A and Thomsen C 2000 *Phys. Rev.* B **61** 5353
[32] Azuhata T, Sota T, Suzuki K and Nakamura S 1995 *J. Phys.: Condens. Matter* **7** L129
[33] Gotz W, Johnson N M, Chen C, Liu H, Kuo C and Imler W 1996 *Appl. Phys. Lett.* **68** 3144
[34] Meister D *et al* 2000 *J. Appl. Phys.* **88** 1811
[35] Skromme B J 1999 *MRS Internet J. Nitride Semicond. Res.* **4** 15

[36] Jayapalan J, Skromme B, Vaudo R and Phanse M 1998 *Appl. Phys. Lett.* **73** 1188
Mireles F and Ulloa S E 1999 *Appl. Phys. Lett.* **74** 248
[37] Fischer S *et al* 1998 *J. Cryst. Growth* **189–90** 556
[38] Rebane Y, Shreter Y and Albrecht M 1997 *Mater. Res. Soc. Symp. Proc.* **468** 179
[39] Fischer S, Wetzel C, Haller E E and Meyer B K 1995 *Appl. Phys. Lett.* **67** 1298
[40] Lagerstedt O and Monemar B 1974 *J. Appl. Phys.* **45** 2266
[41] Kisielowski C *et al* 1996 *Phys. Rev.* B **54** 17 745
[42] Polian A, Grimsditch M and Grzegory I 1996 *J. Appl. Phys.* **79** 3343
[43] Narayan J, Dovidenko K, Sharma A K and Oktyabrsky S 1998 *J. Appl. Phys.* **84** 2597
Shim C J, Kung P, Saxler A, Ohsato H, Harotps K and Razeghi M 1994 *J. Appl. Phys.* **75** 3964
[44] Klemens P G 1966 *Phys. Rev.* **148** 845
[45] Menendez J and Cardona M 1984 *Phys. Rev.* B **29** 2051
[46] Li W S, Shen Z X, Feng Z C and Chua S J 2000 *J. Appl. Phys.* **87** 3332
[47] Di Bartolo B 1968 *Optical Interactions in Solids* (New York: Wiley)
[48] Tsen K T, Joshi R P, Ferry D K, Botchkarev A, Sverdlov B, Salvador A and Morkoc H 1996 *Appl. Phys. Lett.* **68** 2990
Tsen K T, Ferry D K, Botchkarev A, Sverdlov B, Salvador A and Morkoc H 1998 *Appl. Phys. Lett.* **72** 2132
[49] Link A, Bitzer K, Limmer W, Sauer R, Krichner C, Schwegler V, Kamp M, Ebling D G and Benz K W 1999 *J. Appl. Phys.* **86** 6256
[50] Tripathy S, Chua S J, Hao M S, Sia E K, Ramam A, Zhang J, Sun W H and Wang L S 2002 *J. Appl. Phys.* **91** 5840